Development of high speed low noise NIR HgCdTe Avalanche Photodiode Arrays for Adaptive Optics and Interferometry

Gert Finger[a], Ian Baker[b], Reinhold Dorn[a], Siegfried Eschbaumer[a], Derek Ives[a], Leander Mehrgan[a], Manfred Meyer[a] and Jörg Stegmeier[a].
[a]European Southern Observatory, Karl Schwarzschildstrasse 2, D-85748-Garching, Germany.
[b] SELEX Galileo Infrared Ltd, Southampton, Hants, SO15 OLG, UK.

ABSTRACT

The most promising way to overcome the CMOS noise barrier of infrared AO sensors is the amplification of the photoelectron signal directly at the point of absorption inside the infrared pixel by means of the avalanche gain. HgCdTe eAPD arrays with cut off wavelengths of λ_c ~2.64 μm produced by SELEX-Galileo have been evaluated at ESO. The arrays were hybridized to an existing non-optimized ROIC developed for laser gated imaging which has a format of 320x256 pixels and four parallel video outputs. The avalanche gain makes it possible to reduce the read noise to < 7 e rms. The dark current requirements of IR wavefront sensing are also met.

Keywords: avalanche photodiode, eAPD, HgCdTe, readout noise, excess noise. APD gain, cryogenic amplifier, infrared, wavefront sensor, fringe tracker

1. INTRODUCTION

The readout interface circuit (ROIC) of current infrared wave front sensors and fringe trackers is based on CMOS technology. Due to basic limitations of CMOS the improvements of the read noise have been marginal for the last two decades and may be mainly attributed to smaller pixel sizes [1].. The most promising way to overcome the CMOS noise barrier is the amplification of the photoelectron signal directly at the point of absorption inside the infrared pixel by means of the avalanche gain and thence to raise the signal above the noise floor of the focal plane electronics. HgCdTe material having a cut-off wavelength of λ_c>2.3 μm is the ideal detector material since, contrary to silicon, it offers noise free avalanche gain.

For almost a decade now the British company SELEX-Galileo Infrared Ltd has successfully used the eAPD gain in sensors for laser-gated three dimensional (3D) imaging [2,3].The sensors have a cutoff wavelength of 4.5 micron but their dark current is too high for wavefront sensors which typically require integration times of ~ 1ms. Therefore ESO contracted SELEX to develop HgCdTe eAPD arrays having cutoff wavelengths of λ_c ~2.5 μm. The goal of the development was the investigation of the dark current at short cutoff wavelengths and the exploration of the gain, noise and operability parameter space. The eAPD arrays were hybridized to an existing 3D ROIC having a format of 320x256 pixels on 24um pitch with four parallel video outputs. The evaluation of the arrays has shown a classic avalanche gain up to 20 at a 9V bias, a readout noise of < 7 e rms even with non-optimized ROIC's and a dark current compliant with the requirements of AO wavefront sensing. The development of a specific ROIC for AO is expected to deliver the performance goal of a readout noise of less than 3erms at a frame rates of ~ 1kHz.

2. APD GAIN IN MCT

The best semiconductor material for building infrared eAPD arrays is $Hg_{1-x}Cd_xTe$ which has a tunable bandgap. Depending on the stoichiometry x, the cutoff wavelength can be selected. The most promising features of HgCdTe are the uniform APD gain which increases exponentially with the applied bias voltage, the absence of avalanche breakdown and the low excess noise factor F. The excess noise factor is the variance of the detector signal after the APD amplification divided by the product of the variance of the detector signal before APD amplification and the APD gain G. For cutoff wavelengths of λ_c=4.5 μm excess noise factors close to unity have been measured [4]..

The almost ideal APD characteristics of HgCdTe are explained by the much smaller effective mass of the electron compared to that of the hole. The electron ionization coefficient is much larger than the hole ionization coefficient. Therefore, the avalanche gain is only caused by electron avalanching and holes do not contribute to the avalanche gain. The ratio of hole and electron ionization coefficients, k, is low (k ~0) for $\lambda_c > 2.2$ μm material. At shorter cut-off wavelengths holes also contribute to the avalanche effect and the APD gain tends to infinity which is called avalanche breakdown.
The energy band structure of HgCdTe favors noiseless APD gain. Unlike silicon, HgCdTe is a direct semiconductor. The minimum energy of the conduction band is above the maximum energy of the valence band and is not shifted in k-space like it is in silicon, an indirect band gap material. No impulse is needed for an electron to make a transition from the valence to the conduction band. The electrons are accelerated in the electric field of the depletion region and can acquire enough energy for impact ionization without phonon interaction. This process can be described by a pure ballistic ionization model [5]..
Electron injection avalanche photodiode (eAPD) arrays have been in use for laser gated imaging for several years. Three-dimensional imaging is obtained by shooting a collimated λ=1.55 μm laser pulse to illuminate the scene. Depth information is obtained from measurements of the time of flight of the reflected pulse. The distance resolution can be 10s of cm. Typical integration times are 200 ns up to 5μs. The eAPD amplification is used to overcome the fixed noise floor of the CMOS readout multiplexer. Since the integration times are in the nano or microsecond regime, dark current is not an issue and λ_c=4.5 μm HgCdTe can be used. However, for astronomical applications such as wavefront sensing and fringe tracking, integration times are in the millisecond regime and dark current becomes the crucial issue. The shot noise associated with the dark current of λ_c=4.5 μm HgCdTe material limits the sensitivity. Typical dark currents at this cutoff wavelength are ~ 2E-7A/cm^2 and they limit the sensitivity to > 100 electrons rms [4].. Hence shorter cutoff wavelengths have to be used.
For this reason a pre-development study was launched with SELEX to develop wider bandgap material with cutoff wavelengths around λ_c=2.5 μm, in order to investigate whether the reduction of the dark current, which scales exponentially with the bandgap, is sufficient to reach sensitivities of < 5 noise equivalent photons rms for integration times of > 1ms. The APD gain is expected to be smaller for the wider bandgap material but still larger than 10 which is sufficient to meet the sensitivity requirements of infrared wavefront sensing.

3. P-AROUND-N LOOPHOLE DIODES AND MULTIPLEXER

The HgCdTe is grown by liquid phase epitaxy on a CdZnTe substrate, which is then mounted onto the multiplexer. The substrate is then removed. The junctions are not planar structures connected with In bumps to the multiplexer but cylindrical structures with metal vias connecting the junction to the multiplexer. The vias are etched into the p-type substrate using an ion beam etch which creates a cylindrical n+/n region around the via as shown on the left side of Figure 1 [5].. The photons are absorbed in the p region and the electrons diffuse laterally to the depletion region of the pn junction. In the high electric field of the depletion region they are accelerated and get enough energy to generate the avalanche effect by impact ionization. The cylindrical geometry favors the pure electron avalanching.

To keep development costs low the HgCdTe arrays were hybridized to existing multiplexers developed for laser gated imaging. These multiplexers have complicated pixel designs but can be operated in a capacitive discharge mode where the avalanche gain is fully exploited.. The schematics are shown on the right side of Figure 2. The array common sets the avalanche gain. Prior to the integration the anode of the junction is reset to PRV which is 6V. Then the voltage is read by the unit cell source follower when the address switch is activated. At the end of the stare time the voltage is read again and the difference is calculated by the real time preprocessor to obtain the correlated double sample. The array can also be read out nondestructively several times during the stare time to further reduce the readout noise by applying Fowler sampling or follow-up-the-ramp sampling. Since we use 40 MHz ADC's, several digital samples can be taken whilst a pixel is addressed and a digital filter can be applied to these subpixel samples. The maximum number of nondestructive readouts and subpixel samples is limited by the required frame rate. For initial tests we used two multiplexers the ME 770 and the ME784. The ME 770 suffered from readout glow and was replaced by another chip (ME784) which had metal screens to eliminate the glow problem. However, the new device had a maximum bias voltage of 8.2V which prevented us from investigating higher APD gains with the low glow multiplexer. A new silicon batch was run with the protection circuit removed and a new batch of arrays is currently being prepared for delivery and testing at ESO

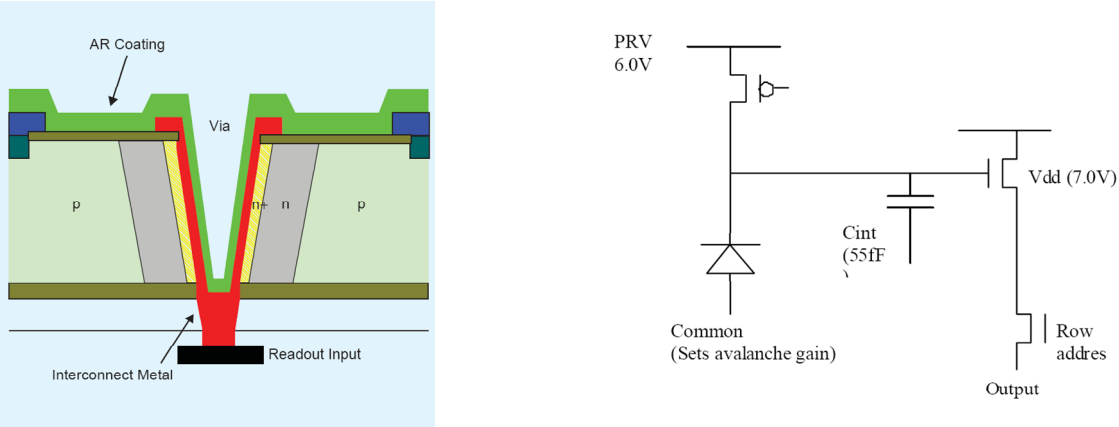

Figure 1 Left: Cross section of cylindrical p-around-n loophole interconnect diode structure. Right: Schematics of multiplexer operated in the capacitive discharge mode

4. CRYOGENIC PREAMPLIFIER

The video signal is amplified directly at the focal plane on the cold detector board shown in Figure 2. A well proven symmetric preamplifier design has been chosen which well matches the differential input stage in front of the ADC on the high speed NGC controller board. The linear CMOS operational amplifier TLC2274 which has a gain-bandwidth product of 2.2 MHz, is too slow for the four 5 MHz video outputs of the ME784 multiplexer. Therefore, it was replaced by the faster OPA354, which also works well at cryogenic temperatures and has a gain-bandwidth product of 100MHz and a noise as low as 6.5 nV/SQRT(Hz). The detector fan-out board with low-pass filters, antistatic protection, cryogenic preamplifiers, flex board and connector is shown on the left side, the design of the symmetric amplifier is shown on the right side of Figure 2

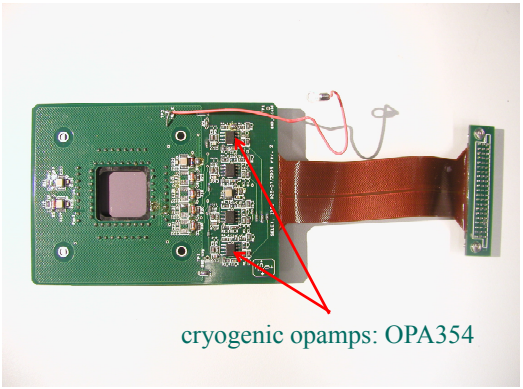

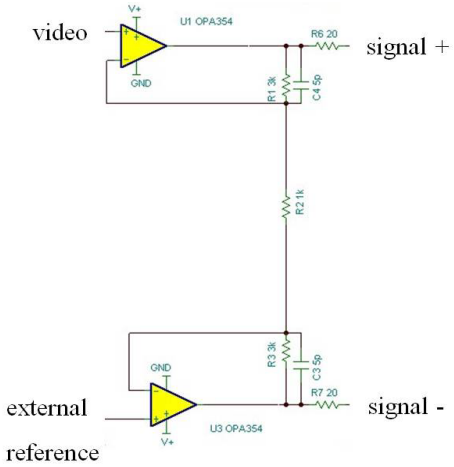

Figure 2 Left: Detector board with low-pass filters, antistatic protection, flex board and cryogenic preamplifiers for four video 5Mz channels of SELEX ME784 multiplexer. Right: Schematics of symmetric cryogenic preamplifier.

One input of the amplifier is the video signal and the other input is an external reference voltage to compensate for the dc offset of the video signal. The amplifier has two outputs, signal+ and signal- , which are routed through the flex board and through external 4 meter long cables to the differential input stage of the high speed NGC controller. The rise time and fall time of the video signal at the ADC input is ~ 80 ns.

5. HIGH SPEED DATA ACQUISITION SYSTEM

To meet the increased speed requirements of low noise high speed infrared detectors deployed in active control loops as wavefront sensors or fringe trackers the standard NGC data acquisition system developed at ESO was enhanced by a high speed derivative of the controller which reuses NGC components as much as possible but employs faster components where required. The whole acquisition system including communication, sequencer, dc and clock level converters, ADC's and telemetry with clock monitors is accommodated on a single printed circuit board of 16x16 cm and consumes 10 W. The new components are the fast clock drivers and fast ADCs which have a 40MHz sample rate. The FPGA architecture based on the VIRTEX II is a copy of the standard NGC controller and includes the implementation of the sequencer. It uses fast serial link technology to establish a fiber link to the pci-bus interface of a Linux preprocessor PC and a serial fpdp link to the real time computer. Register addresses and functions are identical to the Basic Board of the NGC controller.
The high speed board has eight video channels. Each channel is equipped with a 14 bit ADC (AD9248, 2 channels per device) which uses a differential pipelined architecture and digitizes the video signal at a sample rate of 40 MHz. One constraint of a pipeline ADC is that the clock pattern of the detector timing has to be synchronous with the ADC clock. The analog bandwidth of the SELEX APD array is only 5MHz, but the pipeline ADC is continuously sampling at high frequency. To select the correct ADC sample at the exact time when the video signal has settled at a stable voltage which represents the signal of the APD pixel, a "Dummy Convert" strobe is used and a "Convert Delayed" signal is generated in the FPGA to account for the pipeline delay of the ADC. Only the data sampled when "Dummy Convert" is active are acquired and transmitted over the fiber link to the number cruncher PC. The clock drivers can deliver a current of 2A and drive a capacitive load of 1 nF with rise and fall times of 20ns. The bias voltages are programmable and can be set between 0 and 9V. One bias voltage for the array common of the APD's can be set to -4V to allow high reverse bias voltages for high APD gain. The bias voltages can drive 60 mA.

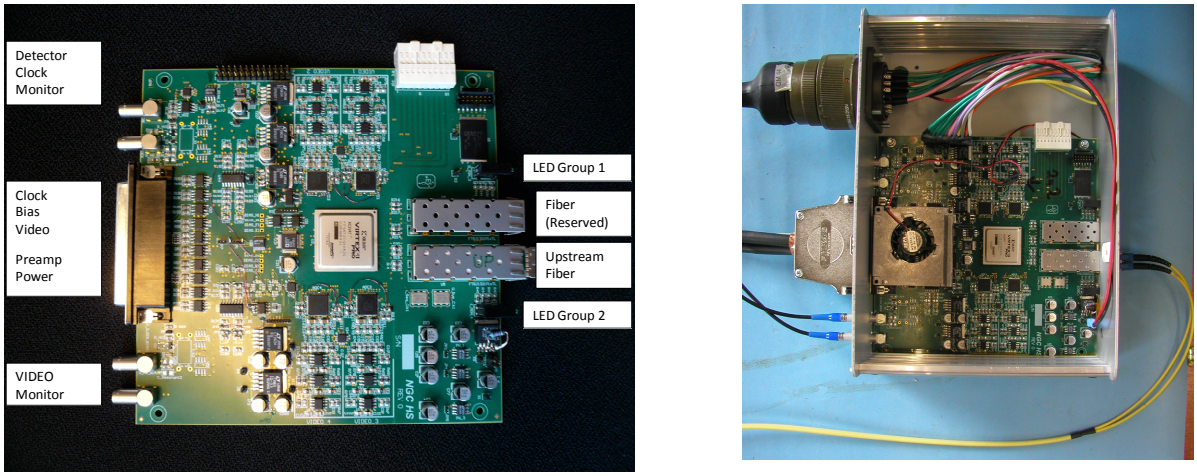

Figure 3 NGC high speed data acquisition system with eight 40 MHz piplined ADC's, ten high speed clocks (rise/fall time 20ns) and 7 bias voltages (-4V/+9V), VIRTEX II FPGA with sequencer and 2.5 Gbit rocket IO fiber link.

6. TEST SETUP

In order to evaluate the performance of the APD array the detector was mounted in the IRATEC test camera which is pre-cooled by liquid nitrogen. The detector can be cooled down to a temperature of 40 K by a closed cycle cooler. The camera optics consists of a cold f/11 Offner relay and two cold filter wheels. One wheel is equipped with bandpass filters and the other wheel with neutral density filters. A test pattern with a grid of holes in front of the camera entrance window is illuminated by an extended blackbody and imaged onto the detector by the Offner relay. By changing the temperature of the blackbody a test pattern of calibrated intensity can be generated and imaged onto the detector as will be shown

below. This allows a comparison of the performance of different detectors in terms of signal to noise without uncertainties due to calibration issues.

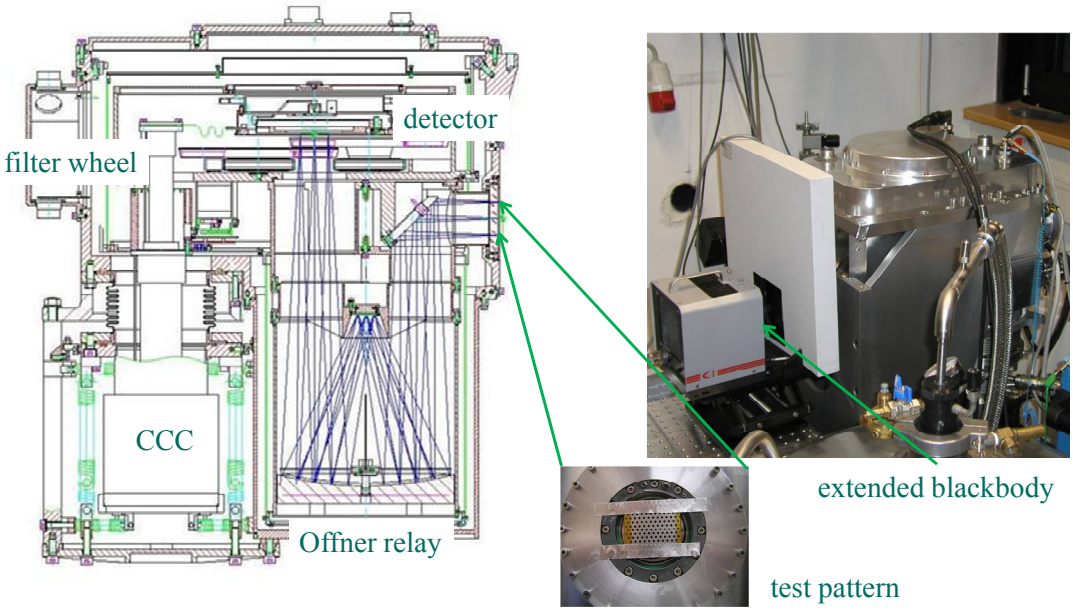

Figure 4 Test setup with IRATEC camera, cold optics and cold filter wheel. Test pattern with grid of holes illuminated by extended blackbody and imaged by f/11 Offner relay onto detector.

7. CONVERSION GAIN AND QUANTUM EFFICIENCY

ESO has received three eAPAD arrays from SELEX for evaluation. The first two arrays were banded arrays with variable junction diameters. The junction diameter is defined by the photoresist and controlled by the voltage of the ion beam milling when cutting the hole in the LPE layer. Smaller junction diameters are preferable because the avalanching is mainly due to electrons which are minority carriers if the photon is absorbed in the p region. In Figure 5 the test pattern with the grid of holes was imaged onto a banded array (#3672-4) which has 6 regions with different junction diameters. Clearly, the region with the smallest junction diameter in the lower left corner of the image shows the best signal to noise ratio.

This area was also used to measure the quantum efficiency of the array in the K-band at a bias voltage of 8.63 V. The conversion gain was determined with the photon transfer curve by measuring the variance versus the signal at different flux levels. The integration time was set to 6.9 ms. The flux was varied by changing the blackbody temperature which illuminated the test pattern. At each temperature a series of 10 exposures was taken. The variance is plotted in Figure 6 as a function of the signal. Assuming that the excess noise factor is close to unity then the inverse slope yields the conversion gain which is 2.46 electrons/ADU. If the excess noise factor is larger than 1 then the inverse slope of Figure 6 has to be increased by the excess noise factor to obtain the correct conversion gain.

The filter transmission of the K-band filter was measured at liquid nitrogen temperature and the solid angle from which the detector pixel accepts radiation is defined by the f/11 Offner relay optics. Changing the blackbody temperature changes the photon flux at the detector which can be calculated to derive the quantum efficiency. In Figure 7 the number of integrated electrons is plotted versus the number of photons yielding a quantum efficiency of 0.7 at a bias voltage of 8.63V.

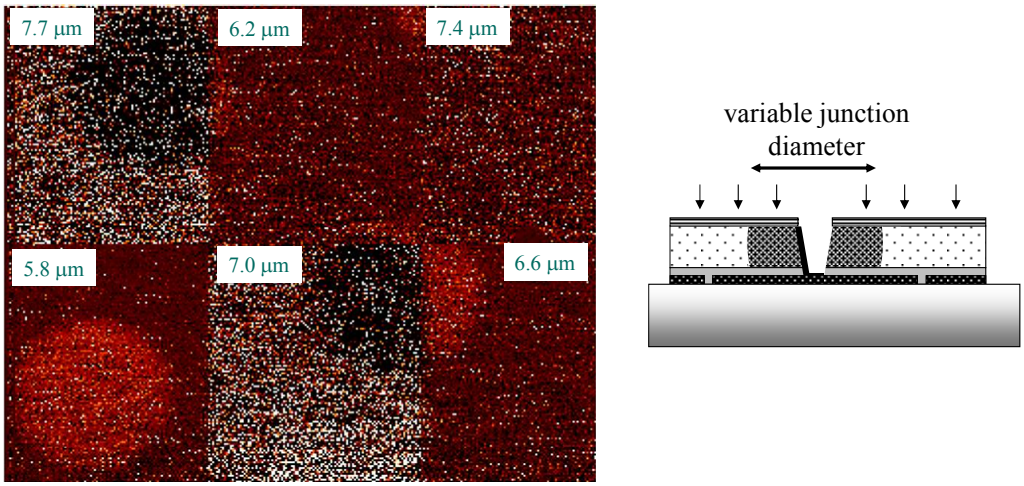

Figure 5 Dependence of image quality on junction diameter of banded array #3672-4 which has six different regions of junction diameters ranging from 5.8 µm to7.7 µm. Smaller junctions are preferable.

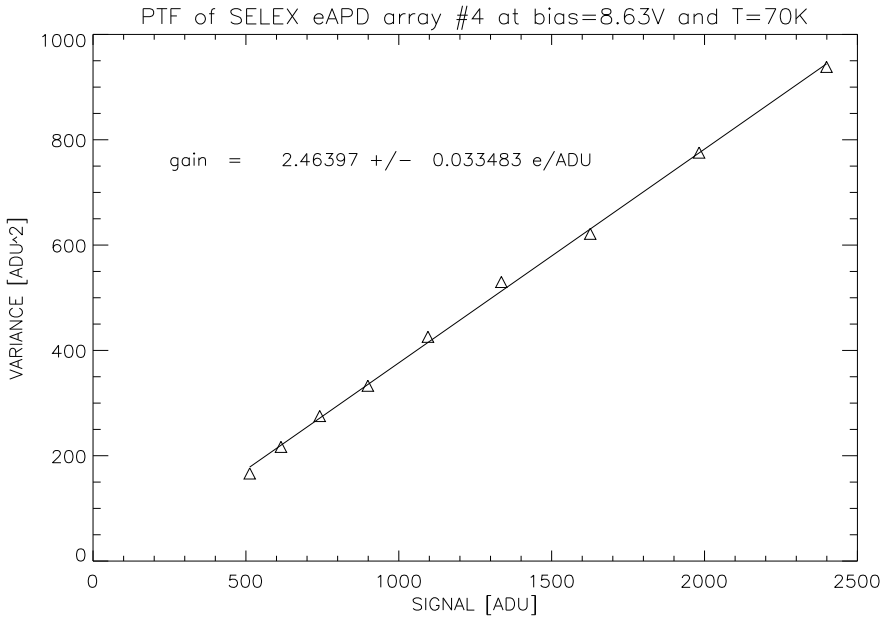

Figure 6 Conversion gain of e APD array #3672-4 at bias voltage of 8.63 V

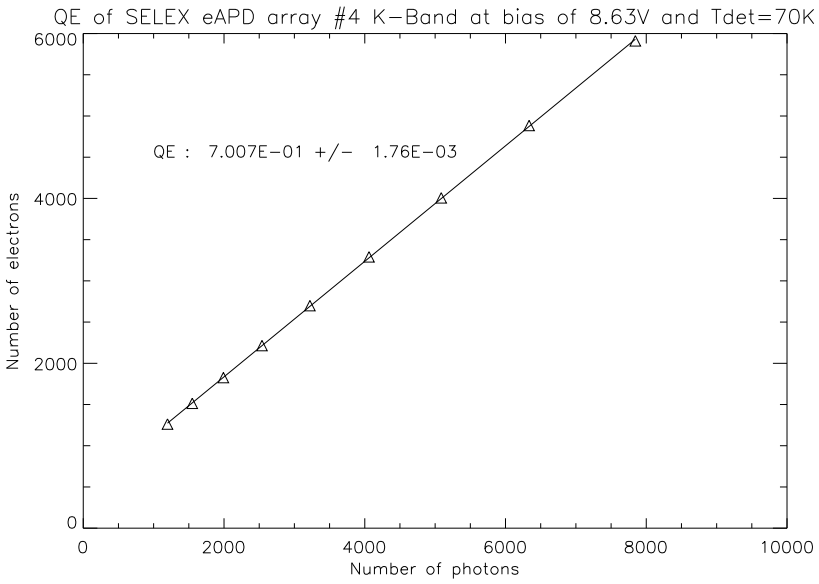

Figure 7 Quantum efficiency of Selex eAPD array (#3672-4) at bias voltage of 8.63 V.

8. APD GAIN

The APD gain was also measured in the region at the lower left corner of array #3672-4 having a junction diameter of 5.8 μm. The blackbody illuminating the test pattern with the grid of holes was set to 125C and the median of the difference of the signal inside and outside the hole of the test pattern was measured at different bias voltages. The measured APD gain versus bias voltage is represented by black diamonds in Figure 8 . The fit to the measured data is shown as a dashed line. The APD gain is 0.0782*2^(2 Vbisa.1.126)+0.905. The model prediction of the APD gain as function of bias voltage for a cutoff wavelength of λ_c=2.65 μm is shown as squares and fits well the measured data. The APD gain at a bias of 8V is 11.6 and rises to 37.7 at a bias of 10 V.

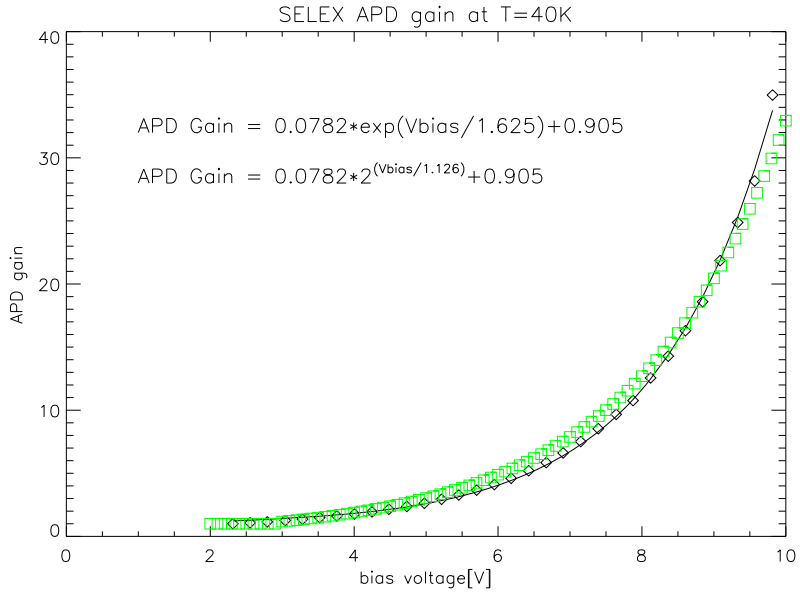

Figure 8 APD gain as function of bias voltage.

9. DARK CURRENT

The most important parameter of wide bandgap HgCdTe eAPD material with a cutoff wavelength of λ_c=2.5 μm is the dark current at high APD gain. A key requirement for the multiplexer of an AO device used in astronomical applications is to minimizes the readout glow. As mentioned above, the first devices (#3672-4 and #3674-6) were hybridized to the multiplexer ME770 which produced about 40 photons per pixel of glow per read out. Hence, the shot noise of the multiplexer glow limited the sensitivity of the array. The source of the glow was a column address MOSFET. Fortunately, another almost pin compatible multiplexer was available which could also be operated in the capacitive discharge mode. This chip (array #4139-04 hybridized to multiplexer ME784) had metal layers which screened the integrating node from the light emitting MOSFET.

To measure the dark current the integrating nodes of the detector pixels were reset and then left floating with the reset switch in the open position. In this way the array was read out 256 times nondestructively as shown by the triangles in Figure 9. The slope of the integration ramp yields the dark current which is 84.5 electrons/s/pixel at a detector temperature of 80K. The dark current measurement was carried out at a bias voltage of 7.8 V with an APD gain of 7.6. Since the conversion gain of 2.2 e/ADU as determined from the photon transfer curve was used to derive the dark current, the value given here represents the dark current referred back to the input before amplification by the avalanche effect. It corresponds to a dark current of 1.2 E-11 A/cm^2 at the output of the detector. The dark current is sufficiently small to allow integrations of up to 10 ms without limiting the sensitivity of the detector. This demonstrates impressively, that widening the bandgap of HgCdTe and using material with a cutoff wavelength of λ_c=2.65 μm brings the dark current down to a level which allows integration times that are long enough to use the APD gain for wavefront sensing and fringe tracking. The sensitivity for typical integration times in the millisecond regime is no longer limited by the shot noise of the dark current.

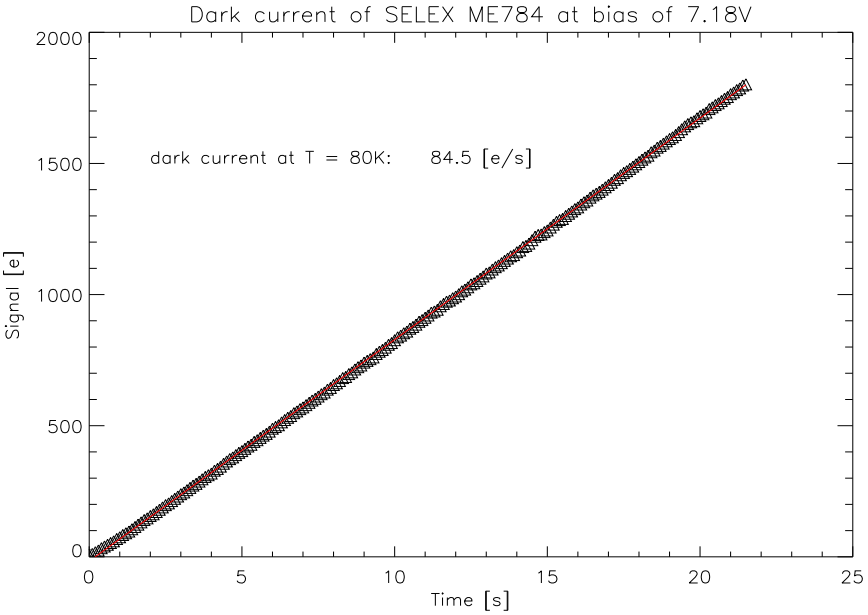

Figure 9 Dark current at T=80 K and bias voltage of 7.18V back-referred to diode input before APD amplification is 84.5 e/s/pixel.

The temperature dependence of the dark current at the output of the detector in units of A/cm^2 is shown in Figure 11. The dark current does not depend on temperature below T=80 K as is to be expected for a dark current process dominated by trap assisted tunneling. However the cosmetics of the APD array improves at lower operating temperatures as demonstrated by the images in Figure 10. Reducing the temperature reduces the number of high dark current pixels. The cosmetic quality is mainly determined by dislocations of the detector material and may also depend on the packaging and thermal stresses. The dark current depends exponentially on the bias voltage as can be seen in Figure 12 [6].. Therefore, it is concluded that the dark current also experiences the avalanche amplification in the high electric field of the diode junction.

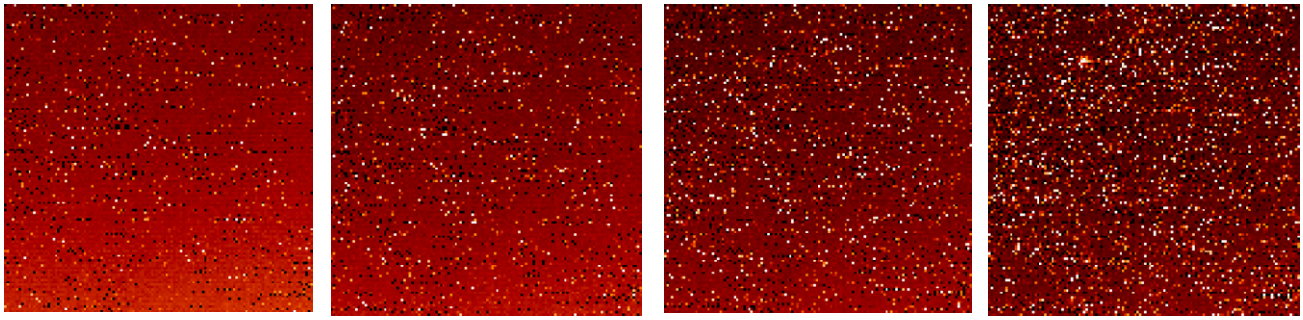

Figure 10 Cosmetic quality of dark frames at different detector temperatures (from left to right: 45K, 60K, 70K, 80K).

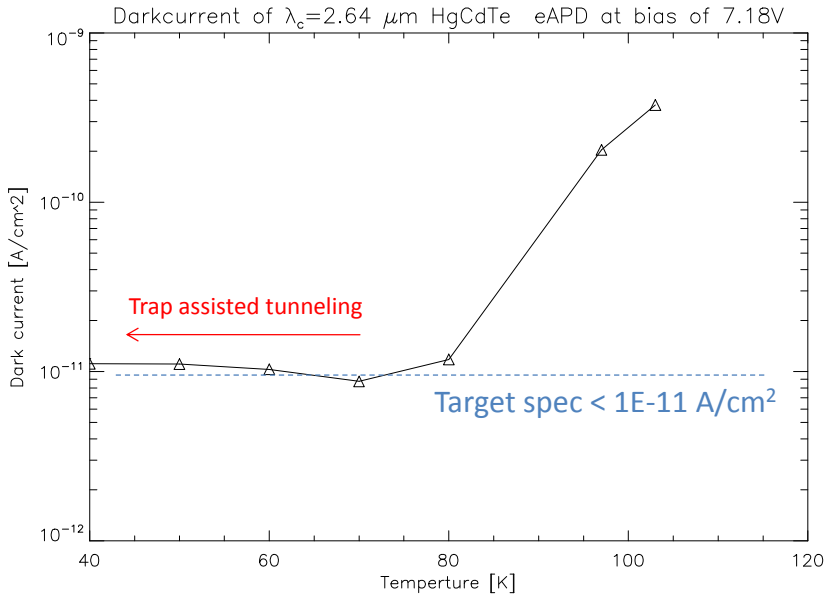

Figure 11 Dark current versus temperature of λ_c=2.64 µm HgCdTe eAPD array at bias voltage of 7.18V. At temperatures below T=80K dark current does not depend on temperature.

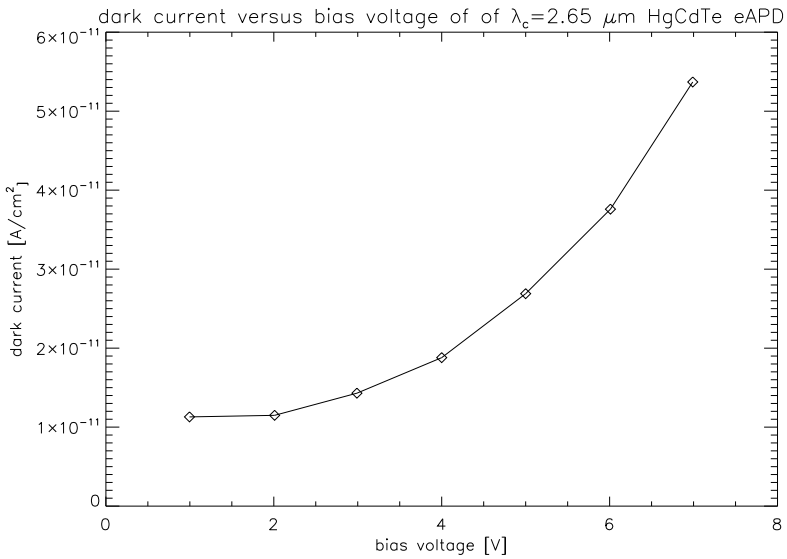

Figure 12 Dark current of λ_c=2.65 μm HgCdTe eAPD array versus bias voltage.

10. READOUT NOISE

The readout noise histogram for double correlated sampling is represented in Figure 13 by the solid line. It was measured with array #4139-04 on multiplexer ME784 at a bias voltage of 7.17V with an integration time of 5.3 ms. The histogram peaks at 7.2 erms. At larger bias voltages with higher APD gain the readout noise is expected to decrease further. But this multiplexer could not be operated at higher bias voltages because of a protection circuit.

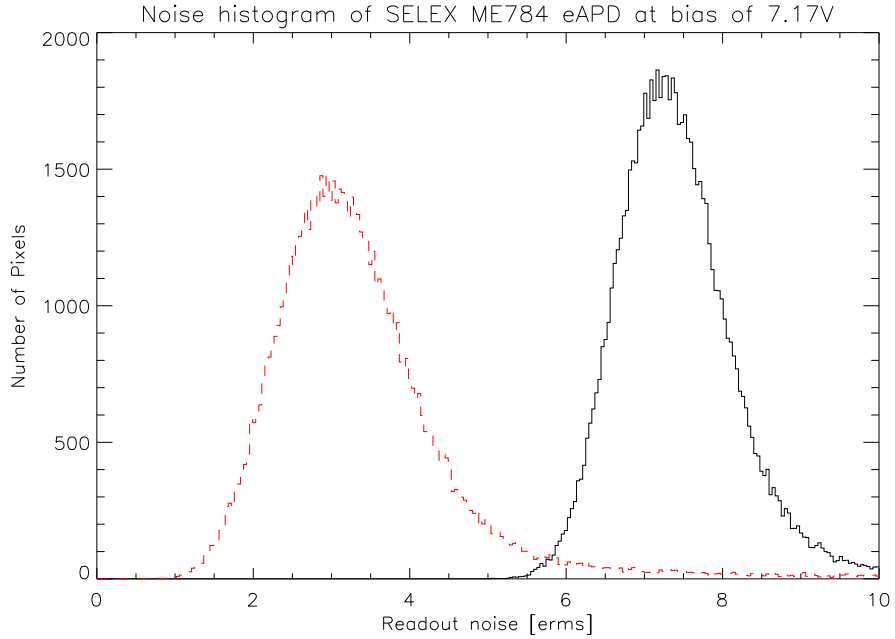

Figure 13 Noise histogram of SELEX eAPD array #4139-03 on ME784 multiplexer at bias voltage of 7.17V. Solid line: double correlated sampling with an integration time of 5.3 ms. Dashed line: 8 Fowler pairs with an integration time of 42 ms.

The readout noise can be further decreased by multiple sampling techniques as shown by the dashed histogram in Figure 13 which represents the readout noise obtained with 8 Fowler pairs and an integration time of 42 ms. It peaks at 2.8 erms. In Figure 14 the readout noise is plotted versus the integration time for an increasing number of Fowler pairs. The number of Fowler pairs varies between one and 64 and is increased in steps by factors of two. As predicted by the dashed line the readout noise decreases by the inverse square root of the number of nondestructive readouts and reaches it's minimum of 2.8 erms for 8 Fowler pairs. For integration times longer than 50 ms the shot noise of the dark current becomes dominant as shown by the dash-dotted line in Figure 14. The combination of readout noise and dark current shot noise shown by the dash-triple-dotted line agrees well with the measured data. Since the conversion gain used for the noise measurements is based on a photon transfer curve measuring the variance versus the signal the assumption is made that the excess noise is close to unity. This assumption still has to be verified for λ_c=2.65 µm material by measuring the excess noise factor F as a function of bias voltage and APD gain.

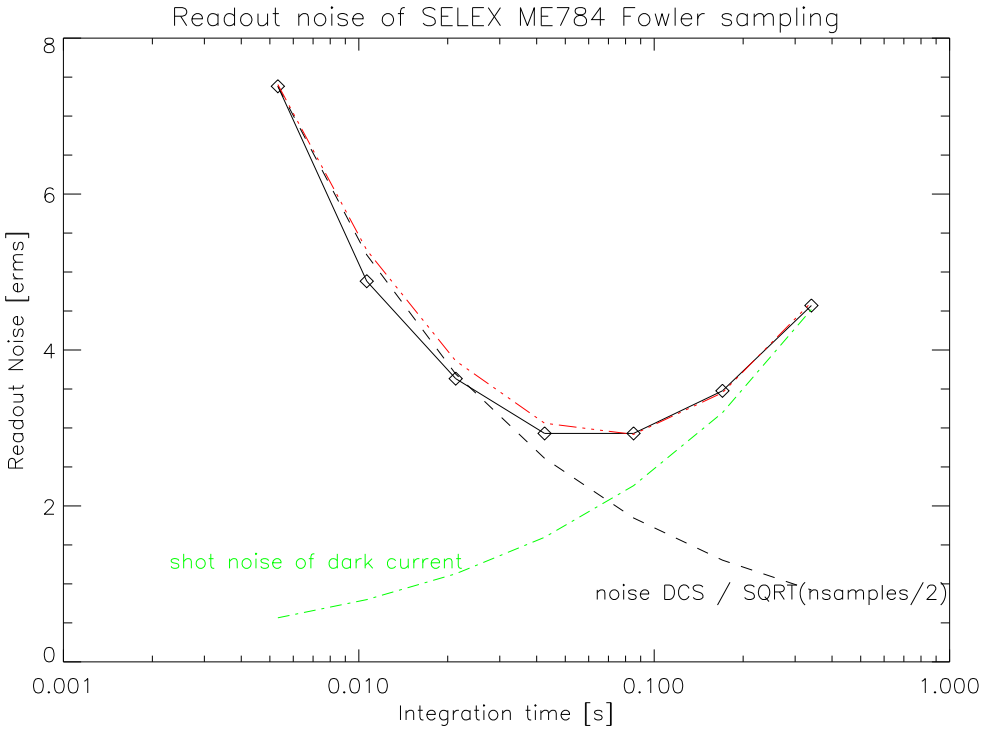

Figure 14 Readout noise versus integration time with Fowler sampling for array #4139-03 on ME784 multiplexer at bias voltage of 7.17V. Readout noise is 3 erms with 8 Fowler pairs. Dashed line: expected noise reduction with Fowler sampling. Dash-dotted line: shot noise of dark current. Dash-triple-dotted line: combination of shot noise and readout noise.

Since the optimization of any detector system aims at maximizing the signal to noise ratio, the grid of holes described in chapter 6 was used to generate a test pattern. The temperature of the blackbody illuminating the test pattern was changed from 25C to 20 C and the difference of the two images is displayed on the left side of Figure 15. The signal difference in the image corresponds to a signal of 6.6 electrons. The integration time was 7.6 ms and the APD gain was 7.3. Without APD gain the test pattern cannot be detected as shown by the right image of Figure 15.

A conventional 256x256 pixel λ_c=2.5 µm HgCdTe CMOS array with 40 µm pixel pitch was used for comparison in the same test setup with the same high speed controller, but slower cryogenic preamplifiers (TLC2274) having a bandwidth of 275 KHz at a gain of 8. The conventional CMOS array was read out at the same speed as the eAPD array, which is too high for its outputs. Hence, the conventional CMOS sensor operates with degraded detector MTF. Since the intensity of the test pattern is uniform and extends over ~ 57 pixels the test pattern can still be seen with blurred edges at an integration time of 6.6 ms if the signal difference is increased from 6.6 electrons/pixel (left image of Figure 16) to 18 electrons/pixel (right image of Figure 16). The test pattern with a signal difference of 6.6 electrons/pixel can be detected by

the APD array operating at an analog bandwidth of 4.5 MHz (left image of Figure 15) but cannot be seen with a conventional CMOS sensor operating at an analog bandwidth of 275 KHz (left image of Figure 16).

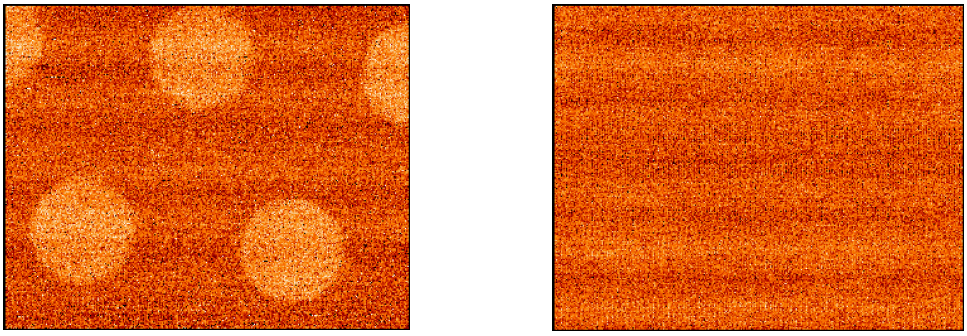

Figure 15 Test pattern observed with eAPD array and single DCS. Average over 10 exposures. Integration time 7.6 ms. Analog bandwidth 4.5 MHz. Signal difference 6.6 electrons/pixel. Left: APD gain=7.34. Right: APD gain 1.

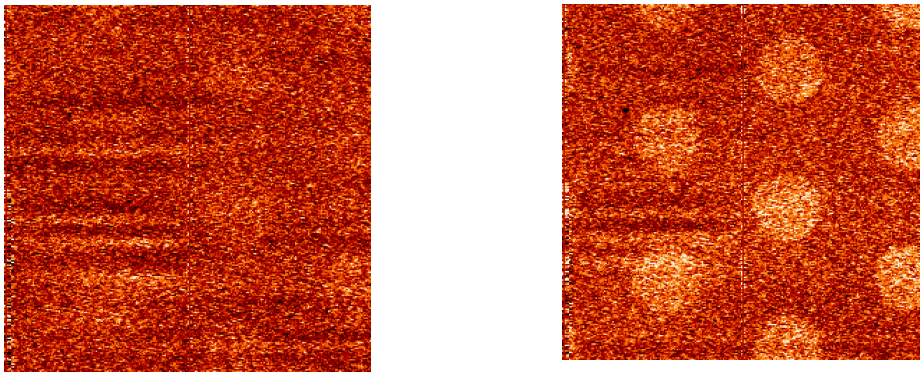

Figure 16 Test pattern observed with conventional CMOS array and single DCS. Integration time 6.6 ms. Analog bandwidth 275 KHz. Average over 10 exposures. Left: signal difference 6.6 electrons/pixel. Right: signal signal difference 18 electrons/pixel.

11. MODEL AND OUTLOOK

By equating the photon generated signal to the total noise which is the quadratic sum of the shot noise and the fixed noise N caused by the CMOS noise floor, 1/f noise and shot noise of the photon background or dark current, the noise equivalent number photons NEP can be derived as given by equation 1[6].. F is the excess noise factor which is close to unity for λ_c = 4.5 μm HgCdTe. QE is the quantum efficiency, C is the capacitance of the integrating node, T the transfer function of the multiplexer from the integrating capacitor to the detector output, e is the charge of the electron and G is the APD gain. If 2NC/TeGF >>1 the NEP is equal to NC/(QE T e G), that is, proportional to the fixed noise N and inversely proportional to the APD gain G. If the APD gain G is high enough to make 2NC/TeGF <<1 the effect of the fixed noise on NEP is eliminated and NEP = F/QE, that is, the only noise is the excess noise F due to APD amplification. An excel model based on equation 1 with experimental data input has been developed to predict the NEP of a custom specific AO multiplexer as a function of bias voltage and is shown in .Figure 17. At a bias voltage of 10 V a noise of 2.3 photons rms is predicted.

$$NEP = \frac{F}{2QE}\left(1+\sqrt{1+\left(\frac{2NC}{TeGF}\right)^2}\right) \qquad \text{EQ (1)}$$

A new readout multiplexer is proposed which is optimized for fringe sensing reading out small stripes of dispersed fringes [7].. The multiplexer shall have 32 video outputs which are organized as 32 sequential pixels in a row. The rows and columns which contain no information are marked by zeros in x and y and are skipped when clocking the detector readout. In this way the full multiplex advantage of 32 parallel outputs can also be exploited when reading small windows. The multiplexer design will consist of a simple source follower with minimum node capacitance in the unit cell. It will be operated in the capacitive discharge mode applying multiple nondestructive readout techniques to reduce the readout noise. With this technique we already obtain a readout noise of 3 erms with the present prototype device.

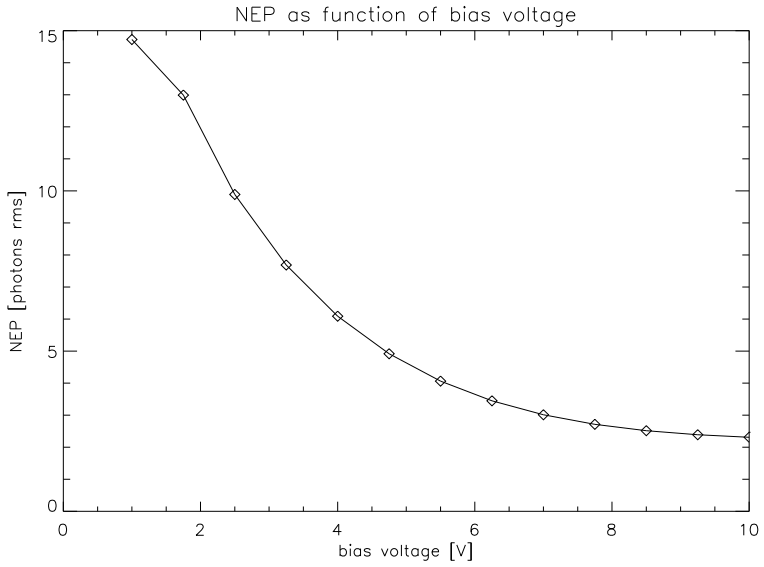

.Figure 17 Model of NEP as function of bias voltage for multiplexer optimized for AO applications.

12. CONCLUSIONS

Changing the cutoff wavelength of HgCdTe from λ_c = 4.5 μm to 2.65 μm decreases the APD gain but also reduces the dark current levels by more than 4 orders of magnitude which is sufficient to deploy eAPDs as high speed low noise infrared wavefront sensors with typical integration times in the millisecond regime. The APD gain opens up the possibility to overcome the CMOS noise barrier which limited the sensitivity of infrared wavefront sensors due to the large bandwidths required to keep the integration times shorter than the coherence time of the atmosphere.

Three λ_c =2.65 μm prototype 320x256 pixel eAPD arrays hybridized to non-optimized multiplexers designed for another application were tested. The arrays had a pixel pitch of 24 μm and four parallel outputs operating at a pixel rate of 5 MHz/s. The dark current back-referred to diode input before APD amplification which was measured with a λ_c = 2.65 μm HgCdTe array hybridized to a low glow multiplexer at a bias voltage of 7.2 V and an APD gain of 7.5 was as low as 85 e/s/pixel. Multiple sampling measurements demonstrated that the shot noise associated with the dark current is negligible for integration times shorter than 40 ms and a readout noise of 2.8 erms can be achieved with 8 Fowler pairs and a readout time of 42 ms. The readout noise for single double correlated sampling is 7.2 erms. The assumption made here is that the excess noise is close to unity but this still has to be verified for λ_c =2.65 μm material. Based on experimental data obtained with the prototype sensors discussed in this paper, a custom specific multiplexer with 32 outputs and windowed readout is expected to meet the noise requirements of fringe tracking and wavefront sensing in an optimum way.

REFERENCES

[1] D.Hall, "Electron-Avalanche and Hole-Avalanche HgCdTe Photodiode Arrays for Astronomy", Workshop Detectors for Astronomy, Garching, (2009). http://www.eso.org/sci/meetings/dfa2009/Presentations/HALL-091015_11.30_GARCHING_ESO_DfA_PRE-FINAL.ppt

[2] I. Baker, S. Duncan, J. Copley, "A low-noise laser-gated imaging system for long-range target identification", Proc. SPIE, Vol. 5406, 133 (2004).

[3] I. Baker, D. Owton, K. Trundle; P. Thorne, K. Storie; P. Oakley and J.Copley," Advanced infrared detectors for multimode active and passive imaging applications", Proc. SPIE 6940, 69402L (2008).

[4] Rothman, J. et al., "HgCdTe APD focal plane array development at CEA LETI Minatec", Proc. SPIE 6940, (2008).

[5] J. Beck; C. Wan, M. Kinch, J. Robinson, P. Mitra, R. Scritchfield, F. Ma, J. Campbell, "The HgCdTe Electron Avalanche Photodiode", PROC SPIE 5564, 44 (2004).

[6] I. Baker, G.Finger, "HgCdTe Avalanche Photodiode Arrays for Wavefront Sensing and Interferometry Applications", Workshop Detectors for Astronomy, Garching, (2009) http://www.eso.org/sci/meetings/dfa2009/Presentations/Baker.ppt

[7] I. Baker, private communication.